1 **Evolution of karst conduit networks in transition from pressurised flow to free**

2 **surface flow**

3

4 **Matija Perne[1,2,3], Matt Covington[3], Franci Gabrovšek [1,*]**

5 [1]{ Karst Research Institute, Research Centre of the Slovenian Academy of Sciences and

6 Arts, Postojna, Slovenia}

7 [2]{ Josef Stefan Institute, Ljubljana, Slovenia}

8 [3]{ Department of Geosciences, University of Arkansas, Fayetteville, USA }

9

10 Correspondence to: F. Gabrovšek (gabrovsek@zrc-sazu.si)

11

Abstract

Most of the existing models of speleogenesis are limited to situations where flow in all conduits is pressurised. The feedback between the distribution of hydraulic head and growth of new solution conduits determines the geometry of the resulting conduit network. We present a novel modelling approach that allows a transition from pressurised (pipe) flow to a free surface (open channel) flow in evolving discrete conduit networks. It calculates flow, solute transport and dissolutional enlargement within each time step and steps through time until a stable flow pattern establishes. The flow in each time step is calculated by calling the EPA Storm Water Management Model (EPA SWMM) , which efficiently solves the 1D Saint Venant equations in a network of conduits. Two basic scenarios are modelled, a Low-dip scenario and a High-dip scenario. In the Low-dip scenario a slightly inclined plane is populated with a rectangular grid of solution conduits. The recharge is distributed to randomly selected junctions. The results for the pressurised flow regime resemble those of the existing models. When the network becomes vadose, a stable flow pathway develops along a system of conduits that occupy the lowest positions at their inlet junctions. This depends on the initial diameter and inlet position of a conduit, its total incision in a pressurised regime, and its alignment relative to the dip of the plane, which plays important role during the vadose entrenchment. In the High-dip scenario a sub-vertical network with recharge on the top and outflow on the side is modelled. It is used to demonstrate the vertical development of karst due to drawdown of the water table, development of invasion vadose caves during vadose flow diversion and to demonstrate the potential importance of deeply penetrating conductive structures.

Key words: Karst, Speleogenesis, Modelling, Storm Water Management Model

1 Introduction

1.1 Speleogenetic models: A short history, aims and results

Karst aquifers are among the most prolific water reservoirs. Due to their heterogeneity and anisotropy, their efficient exploitation and protection face many challenges. The role of solution conduits in karst aquifers has been a topic of numerous studies. Estimates show that conduits carry about 99 % of flow within karst aquifers and present efficient transport pathways for potential pollutants (Worthington, 1999). However, we have only limited insight into karst aquifers; the position of conduit systems is largely unknown, except for the parts accessible for human exploration or encountered directly by drilling or indirectly by geophysical techniques.

Speleogenesis (e.g. the evolution of conduit networks in karst aquifers) has been one of the main topics in karst studies of the last century (Ford and Williams, 2007). Many conceptual models of speleogenesis have been proposed based on field observations (Audra et al., 2007;Ford and Ewers, 1978;Audra and Palmer, 2013;Palmer, 1991) and inference from basic principles of flow. However, to gain insight into the processes governing speleogenesis, different physical models have been built and followed by numerical models that are based on the physical and chemical principles of flow, dissolution and transport.

The main objectives of speleogenetic modelling are to test the conceptual models, to determine and evaluate the role of different geological, hydrological and geochemical factors and to find mechanisms that govern the evolution of conduit networks in karst aquifers. Few examples of direct field application have been published (Epting et al., 2009).

Ewers (1982) applied hardware (physical) models made from plaster of Paris or salt, and discovered several key mechanisms that were later largely confirmed and extended by numerical models. Numerical modelling of single conduit evolution (Dreybrodt, 1990, 1996;Palmer, 1991;Dreybrodt and Gabrovsek, 2000) revealed a feed-back mechanism between flow and dissolution rates and stressed the importance of higher order dissolution kinetics (Dreybrodt, 1990;Palmer, 1991;Dreybrodt, 1996;White, 1977) for the evolution of extended conduits. Such kinetics has been proven experimentally for limestone and gypsum (Eisenlohr et al., 1999;Jeschke et al., 2001). More elaborated models of 2D fractures with statistical aperture fields (Hanna and Rajaram, 1998;Szymczak and Ladd, 2011) showed that nonlinear kinetics is not necessary for the evolution of extended patterns of solution conduits.

3

66   The initial stage of speleogenesis is characterised by slow enlargement of proto-conduits,

67   which is accelerated by positive feedback between flow and dissolution rate under constant

68   head conditions. Dissolutional widening increases the flow rate along an initial fracture. Then

69   as the flow rate increases, fresh aggressive solution penetrates deeper into the fracture and in

70   turn accelerates widening and flow rates. This feedback mechanism leads to *breakthrough*,

71   when flow and widening rate increase by several orders of magnitude in a very short time

72   (Dreybrodt, 1990;Palmer, 1991;Dreybrodt, 1996;Dreybrodt and Gabrovsek, 2000). At

73   *breakthrough* the initiation stage of conduit development ends and the enlargement stage

74   starts. The time needed to reach breakthrough is termed *breakthrough time.*

1.2 Evolution of a discrete network under pressurised flow conditions

76   Individual fractures have been assembled into fracture networks in order to model patterns of

77   evolving conduit systems (Lauritzen et al., 1992;Groves and Howard, 1994;Siemers and

78   Dreybrodt, 1998;Kaufmann and Braun, 2000;Liedl et al., 2003). A typical benchmark setting

79   emerged out of the Ewers's hardware models. It includes a plane populated with initial proto

80   channels (fractures/tubes) with inputs and outputs at different hydraulic heads. These models

81   revealed the competition between different pathways connecting inputs to outputs, as already

82   observed by Ewers (Ewers, 1982;Ford and Williams, 2007) in the physical model.

83   To review some of these basic mechanisms, a simple scenario is shown in Fig.1. It consists of

84   a plane with a rectangular grid of fractures. The boundary conditions are shown on Fig. 1a:

85   the sides of the network are marked geographically N, S, E, W. No-flow conditions are

86   applied on the N and S boundaries. Water enters the network at two inputs, In1 and In2 at the

87   W side, initially at constant head $H = 5000$ cm. The whole E boundary presents output at $H =$

88   0 m. Initial aperture widths of fractures are set to 0.02 cm, except for the fractures along W-E

89   line connecting In 1 to the output boundary, denoted as P1 , which has slightly larger initial

90   aperture (0.03 cm) and evolves faster than P2 (Fig. 1a), which is fed directly by In 2. Figure 1

91   shows aperture widths as line widths and dissolution rates as line colours; the warmer the

92   colour the higher the rate. Equipotential lines are also shown on Figs.1a-f, which show the

93   network at different time stages, denoted in each panel in units of breakthrough time T_B.

94   At 0.99 T_B (Fig. 1a) the high head from the input has penetrated along the widened fractures

95   of P1 deep into the network, and suppressed both the hydraulic gradient and growth of P2.

96   Figure 2 shows the profile of hydraulic head along P1 (dashed) and P2 (full line) at different

4

97   stages, as denoted by arrows. The gradient between the tip of P1 and outputs increases in time
98   until the breakthrough.

99   After breakthrough (Fig. 1b), P1 is widened with the maximum dissolution rate along its
100 entire length. It becomes increasingly uniform and so does the hydraulic gradient along it (see
101 Fig. 1b and Fig. 2). The gradient builds up between the high head region along still pre-
102 breakthrough ("plugged") P2 and post breakthrough ("released") P1, which triggers the
103 growth of conduits connecting P2 to P1. Grey arrows show some principle directions of
104 growth.

105 Two "post-breakthrough" scenarios are envisaged:

106 1) In Fig. 1c and d, the constant head is kept at both inputs. New connections between P2 and
107 P1 evolve, while P2 also grows towards the exit. The network expands along the existing
108 pathways by growth of new bypasses (some are shown by grey arrows) until all possible flow
109 paths evolve (not shown). Of course, all catchments have limits and such conditions cannot
110 last for long.

111 2) In Fig. 1e and f, the recharge at In1 and In2 is limited to Q_{max} = 500 l/s. In this case the
112 constant head conditions break, when inflow at the input reaches Q_{max}. At 1.5 T_B (Fig. 1e), the
113 head at the input of P1 is about 1/5 of h_{max} (see also Fig. 2) and the gradient from P2 towards
114 P1 is high, as In2 is still under maximal head. P2 integrates with P1, but further expansion of
115 network is suppressed as the head along the growing existing pathways decreases in time. The
116 interested reader is referred to a detailed modelling study on the influence of limited discharge
117 upon the resulting distribution of conduit sizes by Hubinger and Birk (2011).

118 *To summarise:* In pressurised flow conditions, the evolution of the network starts with
119 competition of pathways connecting inputs to outputs and continues with their integration and
120 expansion until head gradients along un-evolved pathways are high enough for pathways to
121 breakthrough. The evolution is controlled by the feedback mechanism between the
122 distribution of hydraulic head and growth of new conduit pathways. This interplay is affected
123 by many parameters which reflect local hydrology, geology and geochemistry.

124 Many other scenarios of early speleogenesis have been modelled to study factors such as the
125 role of geochemical conditions and mixing corrosion, exchange flow between the matrix and
126 conduit network, and the role of insoluble rocks in the evolution of conduits (Dreybrodt et al.,
127 2005). Numerical models have been also used to assess increased leakage at dam sites or

5

128   other hydraulic structures where unnaturally high hydraulic gradients cause short
129   breakthrough time (Dreybrodt, 1996;Romanov et al., 2003;Hiller et al., 2011).

130   In real situations the available recharge cannot sustain pressurised flow within the evolving
131   network, and the conduits undergo a transition from pressurised to free surface flow
132   conditions. Most accessible cave systems have undergone such a transition.

133   Though most models have only considered pressurised flow, Annable & Sudicky (1998) and
134   Annable (2003) developed an elaborate model of the evolution of a *single partially filled*
135   *conduit* embedded in variably saturated fractured media under *laminar flow* conditions. The
136   extension of such a model to networks with turbulent flow remains a future challenge.

137   Here we develop a model that goes beyond the dynamics depicted in Fig. 1 by incorporating
138   the transition to, and further evolution in, a free surface flow regime.

1.3 Evolution of karst conduit networks in the vertical dimension

140   The vertical evolution of karst has been under debate for more than a century, starting with
141   classical concepts of Katzer, Grund, Davis, Swinnerton, Rhoads and Sinacori and others
142   (Palmer, 2007). The Four State Model of Ford and Ewers (1978) elegantly combines these
143   concepts and relates cave geometry to the density of permeable fissures.

144   Gabrovšek and Dreybrodt (2001) and Kaufmann (2003) modelled a 2D vertical cross-section
145   of a karst system to explore the evolution of karst aquifers in the dimension of length and
146   depth (*sensu* Ford & Ewers (1978). They have shown the important role of water table
147   drawdown in speleogenesis. These models considered dissolution in the phreatic part of an
148   aquifer only and partly modelled the formation of drawdown vadose passages (Ford,
149   1988;Ford and Williams, 2007). Conceptual models have been developed that hypothesize the
150   diversion of vadose water and formation of invasion vadose systems (Ford, 1988;Ford and
151   Williams, 2007;Palmer, 2007;Audra and Palmer, 2013). However, these conceptual models
152   have not been tested by numerical models.

153   In the following sections we describe how the model is built and present two basic modelling
154   scenarios, each with several representative cases. We focus on the description of new
155   mechanisms of flow pathway selection and discuss the results in view of the existing
156   conceptual models.

2 The model set up

2.1 The conceptual approach

Figure 3 shows a conceptual framework for the modelling presented in this work. We assume a plane populated with conduits with water-soluble walls, similar to that in Fig.1. Water enters the conduit network at selected junctions indicated by arrows in Fig.3. The direct recharge into a junction is limited either by the elevation of the land surface (h_{max}) or by the maximal available recharge Q_{max}; if the hydraulic head is lower than h_{max}, all available recharge (Q_{max}) enters at the junction, otherwise the hydraulic head at the junction is equal to h_{max} and only part of the available recharge enters the system. A similar hardware model was discussed by Ewers (1982) who used the term Multiple-input Multi-rank scenario.

The basic workflow of the model follows the same scheme as in the models cited above (e.g. (Dreybrodt et al., 2005) and includes the following steps:

1. Define the network of conduits and boundary conditions (water inlets and outlets).

2. Calculate flow in the network.

3. Couple flow, dissolution and transport to calculate dissolution rates in all conduits.

4. Change the conduit diameter within a time step according to the dissolution rate and return back to Step 2 or exit the loop when a stable flow pattern is established or no substantial changes in flow pattern are expected.

   We also assume that:

1. The flow does not depend on the dissolved load.

2. Time scales for flow, dissolution and transport can be separated from the timescale for widening, i.e. the evolution goes through a set of stationary states within which the widening is constant.

2.2 The calculation of flow

We assume that the network has passed the initial (inception) stage of speleogenesis and that turbulent flow has already been established in the network. The reader is referred to work of Dreybrodt *et al. (2005)* for early evolution in the laminar flow regime. One-dimensional turbulent flow is considered within all conduits. The flow could be either pressurised or free surface.

7

186   Flow in partially filled conduits is described by Saint Venant equations (Dingman, 2002),

187 which are based on depth-averaged conservation of mass and momentum. Several numerical

188 techniques are used to solve them (Dingman, 2002). Our model invokes an open source

189 package Storm Water Management Model (abbreviated SWMM from here on), developed

190 primarily for flow and transport simulation in sewage systems by the US Environmental

191 Protection Agency (EPA, 2014). SWMM solves the set of Saint Venant equations to the

192 desired approximation and accuracy using successive approximations with underrelaxation

193 (Rossman, 2009). Its use for the simulation of flow in conduit dominated karst systems has

194 been demonstrated by several authors (Peterson and Wicks, 2006;Gabrovšek and Peric,

195 2006;Halihan et al., 1998). The pressurised flow is accounted for by introduction of a

196 fictitious Preissmann slot (Fig. 4) at the top of a conduit's cross-section (Cunge and Wegner,

197 1964). In this way we transform a pressurised pipe to an open channel without considerably

198 changing the hydraulic characteristics and enable use of the same set of equations for both

199 flow regimes. Friction losses in conduits are calculated by the Manning equation

200   (1) $V = \dfrac{k}{n} R^{2/3} S_f^{1/2}$,

201 where S_f is the friction slope, V the flow velocity, R the hydraulic radius (i.e. the ratio

202 between cross-sectional area of flow and wetted perimeter), n the Manning roughness

203 coefficient, here taken in the range $0.01 < n < 0.02$, k a correction factor depending on the unit

204 system used. For the metric system, $k = 1$ m$^{1/3}$/s. By introducing k, n remains dimensionless.

205 SWMM enables easy construction of an arbitrary conduit network and many additional

206 elements, such as reservoirs, catchments etc., which could be implemented into future

207 upgrades of the models presented here.

2.3 Dissolution and transport

209 Dissolution rates in karst environments are determined by the reaction kinetics at the rock-

210 water interface (surface controlled dissolution), by diffusion transport of ionic species

211 between the water-rock boundary and the bulk solution (transport controlled dissolution), and,

212 in the case of carbonates, by the rate of CO_2 hydration (Kaufmann and Dreybrodt, 2007).

213 Each of these mechanisms can be rate limiting under certain conditions.

214 In the early evolution of conduit networks, the water in protoconduits (sub millimetres to few

215 millimetres in size) is close to equilibrium with the mineral being dissolved and dissolution is

8

216 mostly surface controlled, by higher order kinetics in case of limestone and gypsum. In
217 turbulent flow conditions, for cases discussed in this work, dissolution in limestone is
218 dominantly surface controlled by first order kinetics, if the input solution has low saturation
219 ratio. Some issues related to limestone dissolution rates in turbulent flow still remain open;
220 scalloped walls of limestone caves suggest that transport control might play an important role
221 under turbulent flow conditions as well (Covington, 2014).

222 For these reasons we simplify the dissolution kinetics by assuming a linear rate law at the
223 rock-water boundary:

224 (2) $\qquad F_s = \alpha_s (c_{eq} - c_s)$

225 where α_s is the kinetic constant, c_{eq} is the equilibrium concentration of ionic species of the
226 rock forming mineral and c_s their actual concentration at the surface of the mineral. Ions are
227 transported from the surface into the bulk through a Diffusion Boundary Layer (DBL) of
228 thickness ε (Dreybrodt and Buhmann, 1991). The transport rate through the DBL is given by:

229 (3) $\qquad F_t = \alpha_t (c_s - c)$

230 where α_t is

231 (4) $\qquad \alpha_t = D / \varepsilon$.

232 D is a diffusion coefficient, ε the thickness of the diffusion boundary layer and c the
233 concentration in the bulk solution. Equating Eqs. (2) and (3) gives an equation for c_s and an
234 expression for the effective rates:

235 (5) $\qquad F = \alpha(c_{eq} - c); \quad \alpha = \dfrac{\alpha_t \alpha_s}{\alpha_s + \alpha_t}$.

236 α_t depends on the thickness, ε, of the DBL, which is related to the thickness, h, of the viscous
237 sub-layer by Schmid's number (Schlichting and Gersten, 2000):

238 (6) $\qquad \varepsilon = h \cdot Sc^{-1/3}, \ Sc = \dfrac{v}{D}$,

239 where v is kinematic viscosity and Sc the Schmidt number, which represents the relation
240 between the viscous diffusion rate and mass diffusion rate. The thickness of a viscous layer
241 over a flat wall is given by (Incropera and DeWitt, 2002):

9

242 (7) $\quad h = \dfrac{5v}{\sqrt{\tau_\omega / \rho}}$,

243 where τ_ω is viscous shear stress at the wall and ρ is the water density.

244 Viscous shear stress is related to the friction slope S_f

245 (8) $\quad \tau_\omega = \rho g S_f R$,

246 where g is Earth's gravitational acceleration. Taking the Manning relation (Eq. (1)) for S_f and
247 inserting (8) into (7), gives:

248 (9) $\quad h = \dfrac{5v R^{1/6}}{nV}$.

249 Inserting Eq. (9) into Eq. (6) and further into Eq. (4), we get an expression for ε and for the
250 transport constant α_t:

251 (10) $\quad \alpha_t = \dfrac{n \cdot V \cdot D^{2/3} \cdot v^{-2/3}}{5 R^{1/6}}$.

252 Most cases that we present in this work assume that $\alpha_s \gg \alpha_t$, so that $\alpha \approx \alpha_t$. Therefore, the
253 dissolution rates are transport controlled. Usually higher flow rates bring with them stronger
254 mixing, lower bulk concentrations and higher dissolution rates. *In most situations, the rule of*
255 *thumb is: the higher the flow, the higher the dissolution rate.*

256 The ions entering the water increase its saturation state with respect to the mineral forming the
257 walls, and diminish dissolution rates along the flow pathways. The increase of concentration
258 within each conduit is described by a differential equation derived from a mass balance within
259 an infinitesimal segment of conduit:

260 (11) $\quad \dfrac{dc}{dx} = \dfrac{F(x) \cdot P(x)}{Q}$,

261 where *F(x)* is dissolution rate at a coordinate x along a conduit, Q the flow rate and *P(x)*, the
262 conduit's perimeter at x.

10

263   Integration of Eq. (11) along a conduit gives the amount of rock dissolved within the conduit.

264   The dissolved load is added to the downstream junction of the conduit and is then treated as a

265   conservative tracer by the pollutant routing code of SWMM.

266   In most scenarios presented in this work, transport controlled dissolution prevails. Therefore,

267   dissolution rates are dependent on the flow velocity. A case, where the dissolution rates are

268   almost entirely surface controlled, is also presented.

2.4 Dissolutional enlargement

270   Dissolution rates are rates of dissolutional enlargement v in $[LT^{-1}]$. In pressurised conduits,

271   the cross-section changes uniformly during dissolution (Fig. 5). In a time step Δt, a conduit

272   enlarges by $v\Delta t$, while its centre remains at the initial position. For a conduit with a free

273   surface flow, only the wetted part of the wall is dissolved. Therefore, a transition from tube to

274   canyon-like channel is expected. Although SWMM allows arbitrary channel geometries, the

275   tube shape is used also during the vadose conditions in our model. To this extent an

276   approximation is used, where the bottom of a conduit with a free surface flow incises with the

277   true rate v and its radius increases with rate $k\cdot v$, where k is the wetted fraction of the conduit

278   perimeter. The centre of the conduit lowers with the rate $(1-k)v$.

2.5 The model structure

280   Two basic settings are presented: first a model of a *Low-dip* network is presented as

281   conceptually shown in Fig. 3. This scenario is used to examine the evolution of conduit

282   network in a plan view. In a second scenario, a highly inclined *High-dip* network is modelled

283   to explore the vertical organisation of flow pathways, or evolution of the conduit network in

284   dimension of length and depth (*sensu* Ford and Ewers (1978)) .

285   Figure 6 introduces a model structure for the Low-dip network. Circular conduits with length

286   L and initial diameter D are assembled in an inclined rectangular grid. The orientation of the

287   grid plane is marked geographically, N, E, S and W. All conduits are 10 m long, with initial

288   diameters on the order of a few millimetres. Water enters the system through selected

289   junctions indicated by arrows on Fig. 6a and flows out on the eastern boundary. Figure 6b

290   presents junction geometry: each junction is defined by an invert elevation h_0, relative to the

291   base level, an inlet offset h_c, which is the elevation of the conduit inlet relative to the invert

292   elevation, and h_{max}, the maximal depth of water in the junction. If the hydraulic head at a

293   junction is above h_{max}, the junction surcharges.

11

294   Figure 6c shows a side view of the model. The invert elevations increase from E to W, 1 m

295   per junction. The slope of the W-E conduits is therefore 0.1 and N-S oriented conduits are

296   horizontal. The inlet offset defines how much a conduit can incise. To keep conduits from

297   bottoming out as they incise the inlet offsets, h_c, are set to a large value of 100 m. Maximal

298   depth at junctions h_{max} is 120 m for all, except for the input junctions where h_{max} is 111 m.

299   There is no storage at the junctions.

300   Each of the junctions on the E boundary is connected to a large conduit (D = 5 m) that freely

301   drains water to the outfall (see Fig. 6c). These conduits play no role in the network genesis.

302   Their role is to effectively drain all the water arriving to the E junctions. The inverts of these

303   junctions are at the base level and so is the inlet of the outfall conduit. This way the junctions

304   on the E boundary allow a free outflow of the system along that face.

305   In the High-dip model (Figure 7), the slope of the network (and therefore the conduits) is 0.99

306   from top to bottom and 0.1 from left to right. We use the expressions vertical for the steep

307   conduits and horizontal for the gradual ones. Water enters on the top side and exits at the

308   seepage face on the right side. The bottom and left boundaries are impermeable. In all

309   junctions, gradual (horizontal) conduits are positioned 1 m above the steep (vertical) conduits,

310   which assures preferential flow along the vertical plane in vadose conditions (see Fig. 7b).

311   Flow along the horizontal conduits is active only when the junction is flooded above their

312   inlets. The outflow is realised as in the Low-dip case, with large conduits connecting

313   junctions to outfalls on the right boundary.

3 Results

3.1 Low-dip networks

316   We start with a simple scenario where all conduits have the same length (10 m), the same

317   initial diameter (0.005 m) and the same inlet offsets. The network dips from W towards the

318   free outflow boundary on the E side with the slope 0.1 . The model is run for 50 steps of 300

319   s, in total 15 000 s. The rock used is salt.

320   Figure 8 presents six snapshots of the network's evolution. Five inputs with Q_{max} = 1000 l /s

321   are marked by circles and denoted by 1-5 on Fig. 8a. The left column shows flow rates and

322   flow rates are denoted by line thicknesses and flow directions by colour; red

323   represents flow towards N or W and black towards S or E. If the flow is pressurised, the

324   colours are saturated; pale colours denote conduits with free surface flow. The right column

12

represents channel diameters by line thicknesses and growth rates by colours; the warmer the colour the higher the rate of conduit diameter increase. The isolines in the figures represent the total hydraulic heads with numbers given in meters and a contour interval of 1 m. The heads are directly calculated at the junctions and interpolated by kriging elsewhere. Note that equipotential lines for the junctions on the E border are not given, as the conduit leading to the outfall is at the base level and large enough to keep the water in these junctions always low.

Figure 8a shows the initial situation. All inputs are at the maximal hydraulic heads, and only a small part of available recharge enters the network. High gradient drives fast growth of W-E conduits from In1 and In2 (Figs. 8b and 8c). Also, pathways heading N and S from In1 and In2 evolve in the pressurised flow regime. To the west of In1 and In2, the development is still slow, as the potential field flattens towards W. On Fig. 8c, the conduits draining In1 and In2 are pressurised and exhibit large flow and widening rates. The gradients from In3 towards the E boundary build up and drive the evolution of pathways from In3 towards the east. When pathways from In1 and In2 are too large to sustain pressurised flow, the hydraulic head in them drops to their topographic height which attracts additional flow from In3. With further time, the evolution progresses upstream. The flow in pathways draining In4 and In5 also increases; it dominantly follows the straight W-E line, although it is also clearly attracted by vadose pathways leading from In3.

Nevertheless, most of the flow from upstream inputs occurs along a direct line of W-E oriented conduits, which evolve most efficiently (Fig. 8c and d). On Fig. 8e, the In3 has become vadose and in a similar manner now attracts flow from In4 and In5. However, the direct line connecting In4 to the boundary takes most of the flow and grows most efficiently. Figure 8f shows the final stable flow configuration. All the inputs drain the available recharge, with the direct pathways between the inputs and the E boundary being the only ones that contain active flow.

A detailed look at Fig. 8 reveals that at any time, looking at the conduits draining a particular node, the highest flow rates are along W-E conduits, which consequently evolve more efficiently than other conduits. The inlet offsets of W-E conduits incise faster than others and eventually the water level at the junction falls below the lower edges of the other conduits, leaving only the W-E conduits active. This is schematically shown on Fig. 9a, where two outlets from a junction are compared; outlet 1 evolves more during the phreatic stage and,

357 therefore, the bottom of the conduit reaches a lower elevation. Consequently, outlet 1
358 ultimately captures all water during the vadose entrenchment. Several other realisations of this
359 scenario with different recharge rates at the inputs have ended with the same final distribution
360 of active conduits.

361 At this point a short note is needed to explain what is meant by a stable flow configuration. In
362 the case of constant recharge, the configuration is considered to be stable when all junctions
363 are drained by one conduit only, i.e. there are no downstream bifurcations remaining. This is
364 the case in Fig. 8f. In most of the other presented model runs a few outflow bifurcations
365 remain at the last presented timestep. These bifurcations would eventually die out if the
366 model was run long enough. We will use the term quasi-stable to describe such situations.

367 The next step towards less idealised scenarios is to assume that the initial inlet offsets of
368 conduits are randomly distributed within the range of 1 m. Figure 10 shows the network when
369 a *quasi-stable* flow pattern has been established, which is now more complex than in the
370 previous case. The general evolution is similar, progressing upstream, but some N and S
371 oriented conduits may have initial inlets low enough to keep the lowest position until the
372 vadose transition occurs and they capture all the flow from a junction. This is schematically
373 illustrated in Fig. 9b. Figure 11 presents the evolution of a network with initial conduit
374 diameters drawn from a uniform distribution with a range of 10^{-4} m to 10^{-2} m. Initial offsets
375 are the same for all nodes.

376 Generally, the evolution follows the concepts described in Fig. 8. In the pressurised phase, the
377 selection of efficient pathways depends also on the conduit diameters and the W-E conduits
378 are not necessarily the ones with the highest flow rates.

379 Figure 12 shows the evolution of total discharge from the network over time. Initially, most of
380 the available recharge flows over the surface. First In1 and In2 integrate with full recharge
381 summing 2 m^3/s. After the gradient for In3 is increased, In3 integrates and the discharge rises
382 to 3 m^3/s. Then pathways from In4 and In5 start to contribute as these two pathways integrate.

383 Another selection mechanism becomes active at the transition to a free surface flow, which is
384 shown on Fig. 13, where, a few snapshots of the SW part of the network show the evolution
385 of several competing pathways evolving from input In5. The junctions of interest are marked
386 by 1 to 3 and enclosed in grey circles at 4800 s. In the pressurised flow regime (4800 s), the

14

387   N-S oriented conduits, marked by *a*, grow faster than the W-E oriented conduits marked by *b*

388   at all three junctions, because conduits *a* belong to pathways with smaller resistance to flow.

389   When the flow is pressurised, the flow partitioning between two competing pathways,

390   connecting the same junctions is divided based on the resistance to flow. Note that conduits *b*

391   are parallel to the dip of the network, while conduits denoted by *a* are perpendicular to it. The

392   slope of individual conduits and the distribution of slopes along the pathways plays no role.

393   This is not the case in a free surface flow regime, where the slope of the conduit that drains

394   the node is important. When a junction becomes vadose, the flow out of the junction through

395   initially larger, but less steep conduits can be redistributed to more favourable steeper

396   conduits. This leads to downstream redistribution of flow which can make part of the network

397   inactive or change the flow from pressurised to free surface or vice versa in some of the

398   conduits. The described situation is schematically shown on Figure 14, where two pathways,

399   *a* and *b* connect two nodes. Pathway *a* is initially larger, drains more flow, and widens more

400   efficiently in the pressurised phase. When the conduit turns vadose, the flow rates in *a* drop

401   due to the low slope of the channel as it leaves the junction. If, at the transition to free surface

402   flow, the water level in the upstream node has not dropped below the inlet of pathway *b,* the

403   steeper entry into pathway *b* as it leaves the junction causes b to incise faster and

404   progressively capture more flow.

405   Figure 15 presents a quasi-stable flow and network pattern for the case identical to the one

406   presented in Figure 11, but where the plane of the network is additionally tilted from N to S

407   for 0.3 m per node. The tilting makes flow towards S preferential to flow towards N, which is

408   clearly seen in the resulting pattern. The input In4 now joins In3. Because it is near the

409   boundary, the input In5 has no option to develop towards S, except that the pathway heading

410   S from the input (conduit *a* at In5 in Fig.13) now persists much longer.

411   Other scenarios with more complex settings, such as networks with 50 x 50 nodes and

412   networks with irregular recharge, were modelled and additionally confirmed the observations

413   given above.

414   Finally we turn to a network where dissolution rate is dominantly surface controlled, as is

415   supposed to be the case for limestone. To this end we have modelled a network, identical to

416   the one in Fig. 11, but with α_s, c_{eq} and D set so that dissolution rates are several orders of

417   magnitude smaller and almost entirely depend on the saturation state of the solution rather

418   than flow velocity. Since the system is in the post-inception stage the ratio of discharge to

419   flow length (Q/L) in many flow pathways is high enough that they evolve with the maximal

420   growth rates. All conduits and channels along these pathways incise with the same rate. Fig.

421   16 shows the situation at 500 y, when a quasi-stable flow pattern has evolved and the

422   complete network is vadose. All active channels with flow have almost the same inlet offsets

423   and the same incision rates. Note that the colours tell the rate of increase of diameter, which is

424   a product between dissolution rate (which is very uniform in case of surface controlled rates)

425   and the fraction of conduit being flooded. Therefore, colours in this Figure mostly tell how

426   full the conduits are; see also discussion in Section 2.4. The resulting flow pattern is, aside

427   from the initial distribution of diameters and boundary conditions, a consequence of two

428   rules: 1) at each node, channels aligned oriented with the dip drain more flow than channels

429   perpendicular to the dip, 2) if only horizontal channels drain the node, flow is distributed

430   evenly. The presented scenario is highly idealistic and the results and interpretation should be

431   taken with care. In nature, the dissolution rates change with changing lithology, the initial

432   offsets are not even, sediments can play important role, and we may question if purely surface

433   controlled rates are reasonable. However, the model supports the ideas of Palmer (Palmer,

434   1991) , that maze caves develop in situations where Q/L is large along many alternative

435   routes.

3.2 High-dip network

437   We now turn to the situation where the network is steep (almost vertical). As this network

438   presents a vertical cross-section of karst, we omit the geographical notation and use top,

439   bottom, left and right for the sides of the networks.

440   Similar models for laminar flow have been presented by Gabrovsek & Dreybrodt (2001) and

441   by Kaufmann (2003). The basic result of these prior models was a continuous drop of the

442   water table due to increased transmissivity of the network and the formation of base level

443   conduits. If a fixed head boundary was applied, competition between a high conductivity zone

444   along the water table and prominent conduits within the phreatic part of the network resulted

445   in a complex pattern of evolved conduits. For many more scenarios of this modelling

446   approach the reader is referred to the book of Dreybrodt et al. (2005)

3.2.1 The homogenous case with recharge distributed over the top nodes

448   Figure 17 presents a case where all conduits are 10 m long with initial diameter of 0.005 m. A

449   maximum possible recharge of 5 l/s is distributed to all input nodes (blue arrows on Fig. 17a)

450   on the top. The left column shows flow rates as line thicknesses and colours, as denoted in the

16

451 legend, at five different time steps. Although the term "*water table*" might not be applicable

452 for such discrete networks, we will use it for the line along the highest flooded nodes (dotted

453 blue lines in Figs. 17 c and d). The right column shows the conduit diameters as coded in the

454 colour bar for each figure. Equipotential lines in the left column show the distribution of

455 hydraulic head, given in meters.

456 Initially (Fig. 17a), a small part of the available recharge enters the network. At the top-right

457 all the recharge is drained directly into the outfall junction (marked by a red circle on Fig.

458 17a. The flow rates within the conduits are small and dominant along the vertical conduits

459 (top to bottom). Flow along horizontal conduits is small and increases from left to right.

460 After 600 s (Fig. 17 b) the entire network is still pressurised. Horizontal conduits have

461 evolved sufficiently to drain more flow brought in by initially developed vertical conduits.

462 Accordingly, the potential gradient becomes oriented to the right and is highest close to the

463 boundary. Conduits at the top-right corner experience fastest growth and capture almost all

464 recharge from the inputs. The flow in the left part of the network is small and the hydraulic

465 potential field is relatively flat there. After 1200 s (Fig.17 c) the top-right corner has become

466 vadose). In this area, the recharge is carried vertically to the water table. The flow rates are

467 highest along the water table and diminish with distance from it.

468 However, widening is still substantial below the water table which additionally increases the

469 network permeability and downwards retreat of WT. The process continues until the WT

470 drops to the base level and only vertical recharge conduits and a master conduit at the base

471 continue to grow. The vertical conduits have been widened through the entire evolution, the

472 uppermost for the longest time and they are therefore largest. The diameters decrease from top

473 to bottom. On the other hand, the diameter of horizontal channels increase from left to right,

474 as they evolve only below the water table. Therefore, deeper conduits have more time to

475 evolve.

3.2.2 Inhomogeneous case

476

477 In the case shown on Figure 18 we assign a more complex distribution of initial conduit

478 diameters. The initial diameter (d_o) of each conduit is constructed as a sum of a group

479 contribution (d_g) which is given to all conduits aligned along the same line, and an individual

480 contribution (d_i). These are both random, sampled from a uniform distribution, where

481 $d_g \in [0, 0.005 m]$ and $d_i \in [0, 0.01 m]$. The probability that conduits along a certain line get the

482 individual contributions is 0.5. Using this group contribution, we enhance the potential
483 importance of conductive structural lines.

484 The initial diameter of the top horizontal line of conduits is 0.1 m.

485 A recharge of 100 l/s is introduced to the top-left junction (see the blue arrow on Fig. 18a.
486 The two given legends for flow rates and diameters are valid for all figures. At 3000 s (Fig.
487 18a), about one fourth of the available recharge is captured and drained directly to the outfall
488 by the top line of horizontal conduits.

489 Pathways along the conduits with initially larger diameters evolve efficiently and capture an
490 increasing amount of flow.

491 At 9000 seconds (Fig. 18b) about 70% of the flow is captured by the junction marked by a
492 blue triangle and denoted by 1 in Fig. 18b. It feeds a line of vertical conduit that discharge
493 into outflows through horizontal conduits. Numbers on the conduits in the top-right region
494 denote flow along the conduits in l/s. The discharge to the outflow diminishes downwards.
495 However, these conduits widen effectively and cannot sustain a pressurised regime, so that the
496 position of highest outflow migrates downwards.

497 By 24000 s, the outflow position has retreated to the bottom (Fig. 18c). When the vertical
498 pathway downwards from point 1 becomes vadose, it provides a free outflow boundary and
499 triggers the development of pathways draining sink points 2 and 3 (Fig. 18b,c), which soon
500 capture all the flow. On Fig. 18c, the flow along the top line has retreated to point 3 and
501 throughout the remainder of the simulation continues to retreat towards the left to points 4 and
502 5 (Fig. 18d) . Ultimately, the flow is captured by the node at point 5 (Fig. 18e). Similarly, the
503 flow migrates from top to bottom, towards the deeper connecting pathways. Figure 18e shows
504 the stable flow situation at 75000 s, where all the flow follows one single pathway.
505 Downward and leftward progress is slow because some of the conduits to the left are initially
506 small and the permeability is low. In comparison with a uniform network with distributed
507 recharge, the development follows initially prominent pathways, with progressive upstream
508 flow capturing. Soon after a pathway becomes vadose, the flow is overtaken by the evolving
509 pathways to its left.

3.2.3 The role of prominent structures

The progression mechanism described above, is demonstrated clearly by a final idealised, but telling, example. We assume three vertical conduits ("wells") with an initial diameter of 0.2 m, extending completely through the domain in the vertical direction.

These are connected with 5 evenly spaced horizontal conduits with initial diameter 0.005 m extending across the domain. All other conduits are effectively impermeable, with a diameter of 10^{-5} m. A maximum possible recharge of 100 l/s is available to the prominent vertical conduits (wells) as marked by the arrows at the top of Figure 19a.

Initially (Fig. 19a), all conduits are pressurised. There is almost no gradient left of W3, where evolution is slow or none. High gradients exist between W3 and the outfalls, the highest being along the deepest horizontal conduit, which has the highest flow and evolves most efficiently. As W3 becomes vadose, it presents a free outflow boundary for the flow from its left and the gradient along the horizontal conduits connecting W2 to W3 builds up. These conduits now experience fast evolution with rates increasing from the top to the bottom (Fig. 19b). The mechanism progresses leftwards: when W2 becomes vadose, W1 connects to it as shown in Fig 19c. In Figure 19d, a stable flow condition is shown, where all the flow follows the wells which feed the base level channel.

4 Discussion

4.1 Low-dip scenario

Sensu Palmer (2007) this paper considers the hydrological control of cave patterns, particularly those leading to branchwork cave systems. In the pressurised phase the model gives similar results as the other existing models. This model introduces the selection of flow pathways on a local scale, i.e. at a particular junction, which occurs when a junction becomes vadose. In a long term perspective, only one outlet conduit drains the node. In nature, down-flow bifurcations are not common in open channels.

In the pressurised phase, the flow out from a junction is distributed to the outlet conduits, according to their resistance to flow and the distribution of hydraulic heads. This also defines the rate of their inlet incision. When a junction becomes vadose, the conduit with the lowest inlet entry elevation has an advantage and is a candidate to take all the flow. However, under vadose conditions the conduit's alignment with respect to the dip of the network becomes

19

important, as higher slope generally invokes higher energy grade, higher flow velocity and faster incision. A conduit that gains advantage in pressurised conditions, can be surpassed by a conduit with a higher slope, which has an advantage in free surface conditions. Once the stable flow pattern is established, the flow follows a system of conduits that all occupy the lowest position in their upstream junctions.

4.2 High-dip scenario

In a homogenous scenario, the evolution is focused to the transitional area between pressurised and free surface flow, the "water table". The flow from the surface is gravitational along the vadose channels down to the water table. There, it is largely focused to the conduits close to the water table. The scenario demonstrates a relatively smooth drawdown of the water table due to increasing permeability in the phreatic zone. The end result is a relatively uniform network with a growing base level conduit. Similar results were obtained by Gabrovšek and Dreybrodt(2001) and by Kaufmann (2003), where only dissolution in the phreatic zone was considered.

The inhomogeneous case demonstrates the evolution of invasion vadose caves based on flow diversion. The drawdown of the phreatic zone is irregular, following fast evolution of prominent pathways and progressive upstream flow capturing. Such a scenario can produce extended an network of steep vadose passages.

Deeply penetrating conductive structures can play an important role as they transfer surface water deep into the massif and redistribute hydraulic gradients. This way fast evolution along deep horizons can be triggered.

5 Conclusion

The presented model closes some of the open questions, which have not been addressed by the older existing models. The final flow pattern results from all stages of network development, starting with the initial stage, continuing with the growth, integration and expansion under pressurised flow and, what is demonstrated by this model, with the final selection of stable flow pathways on a local scale during and after transition to free surface flow regime.

On the other hand the model opens new challenges related to evolution of karst aquifers in vadose settings. Further work is needed to improve estimation of dissolution rates and the

20

570 related role of sediment transport and mechanical erosion. Further steps towards more realistic
571 modelling domain and boundary conditions are also needed. In fact, a single low-dip plane is
572 a scenario, which is not common in the nature. A *careful* step towards 3D models that
573 simulate speleogenesis in both, phreatic and vadose conditions is therefore needed. By
574 careful, we mean gradual adding of complexity, so that at each new step all mechanisms from
575 previous steps are well understood. The presented model allows such extensions.

576 At the same time, we have to keep in mind the modelling results are not stand-alone, they
577 should progress hand in hand with conceptual models based on the field observations.

583

21

References:

Annable, W. K., and Sudicky, E. A.: Simulation of karst genesis: hydrodynamic and geochemical rock-water interactions in partially-filled conduits, Bulletin d'Hydrogeologie, 16, 211-221, 1998.

Annable, W. K.: Numerical analysis of conduit evolution in karstic aquifers, Ph.D, University of Waterloo, 139 pp., 2003.

Audra, P., Bini, A., Gabrovsek, F., Hauselmann, P., Hoblea, F., Jeannin, P., Kunaver, J., Monbaron, M., Sustersic, F., Tognini, P., Trimmel, H., and Wildberger, A.: Cave and karst evolution in the Alps and their relation to paleoclimate and paleotopography, Acta Carsologica, 36, 53-67, 2007.

Audra, P., and Palmer, A. N.: 6.17 The Vertical Dimension of Karst: Controls of Vertical Cave Pattern, in: Treatise on Geomorphology, edited by: Shroder, J. F., Academic Press, San Diego, 186-206, 2013.

Covington, M. D.: Calcite dissolution under turbulent flow conditions: a remaining conundrum, Acta Carsologica, 43, 159-202, 2014.

Cunge, J. A., and Wegner, M.: Numerical integration of Barré de Saint-Venant's flow equations by means of an implicit scheme of finite differences., La Houille Blanche., 33-39, 1964.

Dingman, S. L.: Physical hydrology, Prentice Hall, Upper Saddle River, N.J., 646 pp., 2002.

Dreybrodt, W.: The role of dissolution kinetics in the development of karst aquifers in limestone - A model simulation of karst evolution, Journal of Geology, 98, 639-655, 1990.

Dreybrodt, W., and Buhmann, D.: A Mass-Transfer Model For Dissolution And Precipitation Of Calcite From Solutions In Turbulent Motion, Chemical Geology, 90, 107-122, 1991.

Dreybrodt, W.: Principles of early development of karst conduits under natural and man-made conditions revealed by mathematical analysis of numerical models, Water Resources Research, 32, 2923-2935, 1996.

Dreybrodt, W., and Gabrovsek, F.: Dynamics of the evolution of a single karst conduit, in: Speleogenesis: Evolution of karst aquifers, edited by: Klimchouk, A., Ford, D. C., Palmer, A., and Dreybrodt, W., National Speleological Society, 184-193, 2000.

Dreybrodt, W., Gabrovsek, F., and Romanov, D.: Processes of speleogenesis: A modeling approach, Carsologica, edited by: Gabrovsek, F., Založba ZRC, Ljubljana, 375 pp., 2005.

Eisenlohr, L., Meteva, K., Gabrovsek, F., and Dreybrodt, W.: The inhibiting action of intrinsic impurities in natural calcium carbonate minerals to their dissolution kinetics in aqueous H_2O-CO_2 solutions, Geochimica Et Cosmochimica Acta, 63, 989-1001, 1999.

Storm Water Management Model (SWMM): http://www.epa.gov/nrmrl/wswrd/wq/models/swmm/, access: 23.09.2014, 2014.

Epting, J., Romanov, D., Huggenberger, P., and Kaufmann, G.: Integrating field and numerical modeling methods for applied urban karst hydrogeology, Hydrol. Earth Syst. Sci., 13, 1163-1184, 10.5194/hess-13-1163-2009, 2009.

Ewers, R.: Cavern development in the dimension of length and breadth, McMaster University, 1982.

Ford, D. C., and Ewers, R.: The development of limestone caves in the dimensions of length and depth, Canadian Journal of Earth Sciences, 15, 1783-1798, 1978.

Ford, D. C.: Characteristics of dissolutional cave systems in carbonate rocks, in: Paleokarst, edited by: James, N. P., and Choquette, P. W., Springer, New York, 25-57, 1988.

Ford, D. C., and Williams, P.: Karst Hydrogeology and Geomorphology, John Wiley & Sons, Chichester, 562 pp., 2007.

Gabrovšek, F., and Dreybrodt, W.: A model of the early evolution of karst aquifers in limestone in the dimensions of length and depth, Journal of hydrology, 240, 206-224, 2001.

Gabrovšek, F., and Peric, B.: Monitoring the flood pulses in the epiphreatic zone of karst aquifers: The case of Reka river system, Karst plateau, SW Slovenia, Acta carsologica, 35, 35-45, 2006.

Groves, C. G., and Howard, A. D.: Early development of karst systems.1. Preferential flow path enlargement under laminar-flow, Water Resources Research, 30, 2837-2846, 1994.

Halihan, T., Wicks, C. M., and Engeln, J. F.: Physical response of a karst drainage basin to flood pulses: Example of the Devil's Icebox cave system (Missouri, USA), Journal Of Hydrology, 204, 24-36, 1998.

Hanna, R. B., and Rajaram, H.: Influence of aperture variability on dissolutional growth of fissures in karst formations, Water Resources Research, 34, 2843-2853, 1998.

Hiller, T., Kaufmann, G., and Romanov, D.: Karstification beneath dam-sites: From conceptual models to realistic scenarios, Journal of Hydrology, 398, 202-211, http://dx.doi.org/10.1016/j.jhydrol.2010.12.014, 2011.

Hubinger, B., and Birk, S.: Influence of initial heterogeneities and recharge limitations on the evolution of aperture distributions in carbonate aquifers, Hydrol. Earth Syst. Sci., 15, 3715-3729, 10.5194/hess-15-3715-2011, 2011.

Incropera, F. P., and DeWitt, D. P.: Fundamentals of heat and mass transfer, J. Wiley, New York, 981 pp., 2002.

Jeschke, A. A., Vosbeck, K., and Dreybrodt, W.: Surface controlled dissolution rates of gypsum in aqueous solutions exhibit nonlinear dissolution kinetics, Geochimica et cosmochimica acta, 65, 27-34, 2001.

Kaufmann, G., and Braun, J.: Karst aquifer evolution in fractured, porous rocks, Water Resources Research, 36, 1381-1391, 2000.

Kaufmann, G.: Modelling unsaturated flow in an evolving karst aquifer, Journal Of Hydrology, 276, 53-70, 2003.

Kaufmann, G., and Dreybrodt, W.: Calcite dissolution kinetics in the system $CaCO_3$-H_2O-$CaCO_3$ at high undersaturation, Geochimica Et Cosmochimica Acta, 71, 1398-1410, 2007.

Lauritzen, S.-E., Odling, N., and Petersen, J.: Modelling the evolution of channel network in carbonate rocks, ISRM Symposium: Eurock '92, 1992, 57-62,

Liedl, R., Sauter, M., Huckinghaus, D., Clemens, T., and Teutsch, G.: Simulation of the development of karst aquifers using a coupled continuum pipe flow model, Water Resources Research, 39, art. no.-1057, 2003.

Palmer, A. N.: Origin and morphology of limestone caves, Geological Society of America Bulletin, 103, 1-21, 1991.

Palmer, A. N.: Cave geology, Cave Books, Dayton, Ohio, vi, 454 p. pp., 2007.

Peterson, E., and Wicks, C.: Assessing the importance of conduit geometry and physical parameters in karst systems using the storm water management model (SWMM), Journal of Hydrology, 329, 294-305, 2006.

Romanov, D., Gabrovsek, F., and Dreybrodt, W.: Dam sites in soluble rocks: a model of increasing leakage by dissolutional widening of fractures beneath a dam, Engineering Geology, 70, 17-35, 2003.

Rossman, L. A.: Storm Water Management Model, Version 5.0, US Environmental Protection Agency, Cincinnati, 266 pp., 2009.

Schlichting, H., and Gersten, K.: Boundary-Layer Theory, 8th ed., 802 pp., 2000.

Siemers, J., and Dreybrodt, W.: Early development of karst aquifers on percolation networks of fractures in limestone, Water Resources Research, 34, 409-419, 1998.

Szymczak, P., and Ladd, A. J. C.: The initial stages of cave formation: Beyond the one-dimensional paradigm, Earth Planet. Sci. Lett., 301, 424-432, 2011.

White, W. B.: The role of solution kinetics in the development of karst aquifers, in: Karst Hydrogeology, Memoir 12, edited by: Dole, F. L., and Tolson, J. S., International Association of Hydrogeologists, 503-517, 1977.

Worthington, S.: A comprehensive strategy for understanding flow in carbonate aquifers, in: Karst modeling: Special publicattion 5, edited by: Palmer, A., Palmer, M., and Sasovsky, I., The Karst Waters Institute, Charles town, West Virginia, 30-37, 1999.

Table:

Parameter	Notation	Value	Units
Diffusion coefficient	D	$1.5 \cdot 10^{-9}$ salt $1 \cdot 10^{-9}$ limestone	m^2/s
Manning roughness coefficient	n	0.01 or 0.015	1
Surface rate constant	α	1 salt $2 \cdot 10^{-7}$ limestone	m/s
Volume Equilibrium concentration	c_{eq}	0.166 salt $1.1 \cdot 10^{-4}$ limestone	1*
Gravitational acceleration, Density	g,ρ	9.81	m/s^2
Density of water	ρ	10^3	kg/m^3
Dynamic Viscosity of water	μ	10^{-3}	Pa·s

683

684 Table 1: List of rate constants and other parameters used in this work. * To have dissolution
685 rates expressed as a velocity of wall retreat, concentration $[NL^{-1}]$ is multiplied with molar
686 mass $[MN^{-1}]$ and divided by the density $[ML^{-3}]$ of the mineral forming the rock and being
687 dissolved. This makes c_{eq} it dimensionless.

688

24
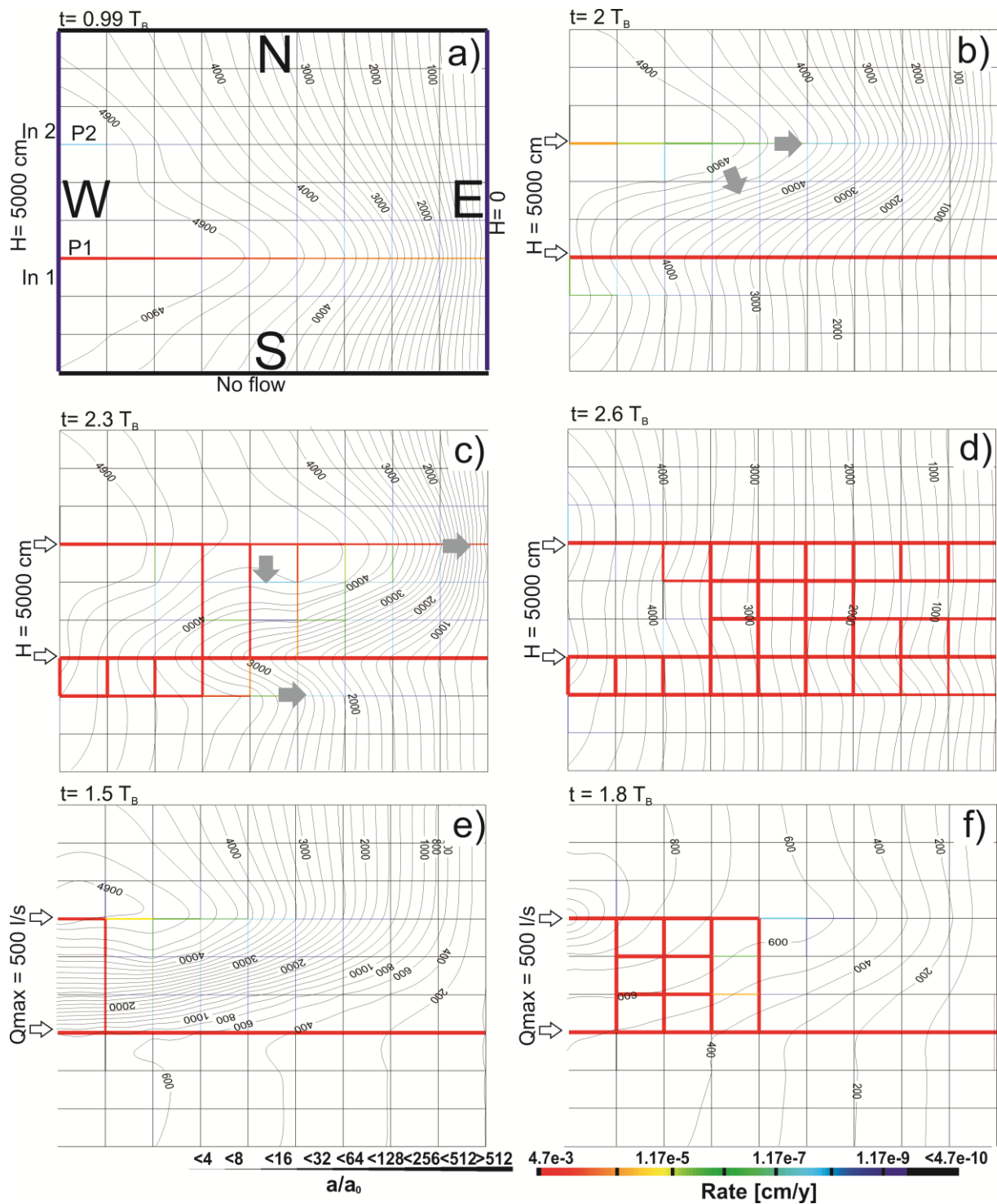
691   Figure 1: Evolution of 2D fracture network under pressurised flow. Panels show aperture
692   widths and dissolution rates at different stage of evolution. Size of the domain is 1 km x 1 km,
693   initial aperture width $a_0 = 0.02$ cm, except for the line P1 , where $a_0 = 0.03$ cm. Linear and
694   forth order dissolution kinetics for the limestone is used (see Dreybrodt et al. (2005) for
695   details).

25

696
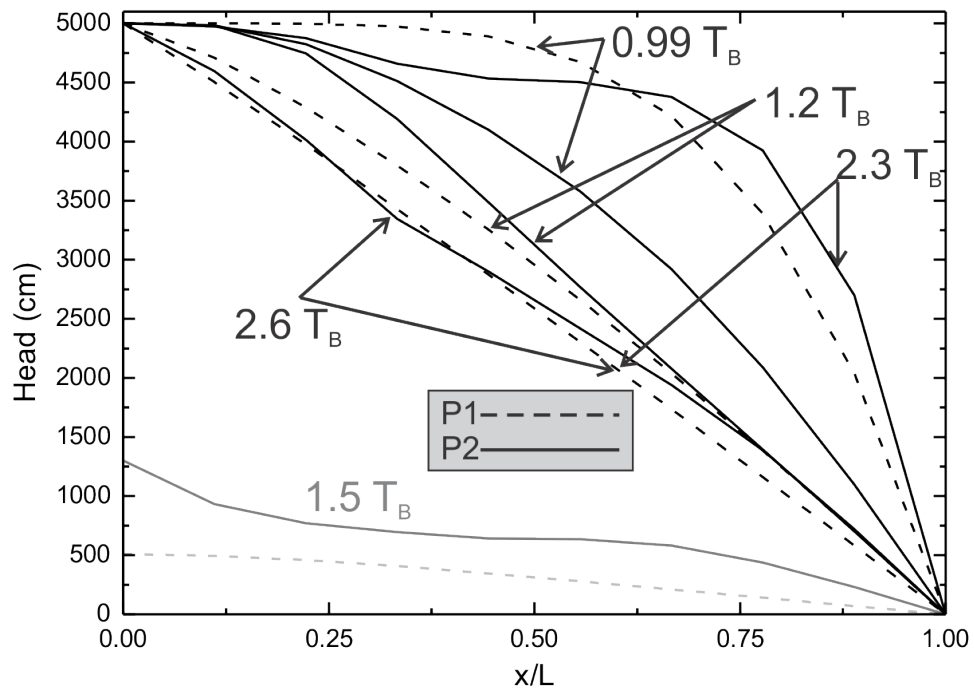
697

698   Figure 2: Profile of hydraulic head along pathways P1 (dashed lines) and P2 (full lines) from
699   Fig.1. Profiles are taken at different time steps, given in units of breakthrough time (T_B).
700   Grey lines show scenario with constant input at $1.5T_B$ (Fig.1e).

701

702

703
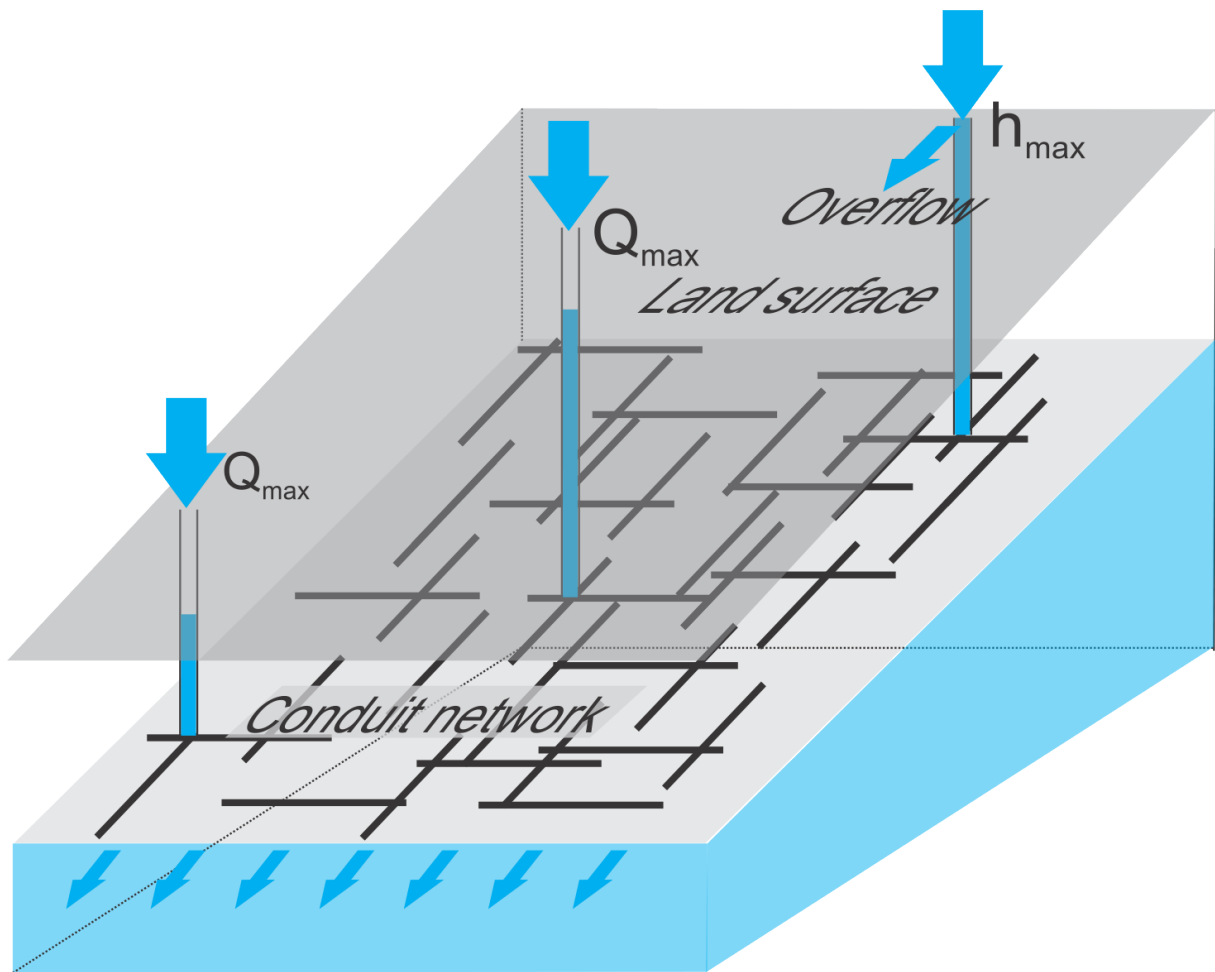
Figure 3: Conceptual framework. A conduit network with point recharge at selected locations indicated by arrows. Recharge is limited by the position of the land surface h_{max} or by maximal available recharge Q_{max}.

708

709

27
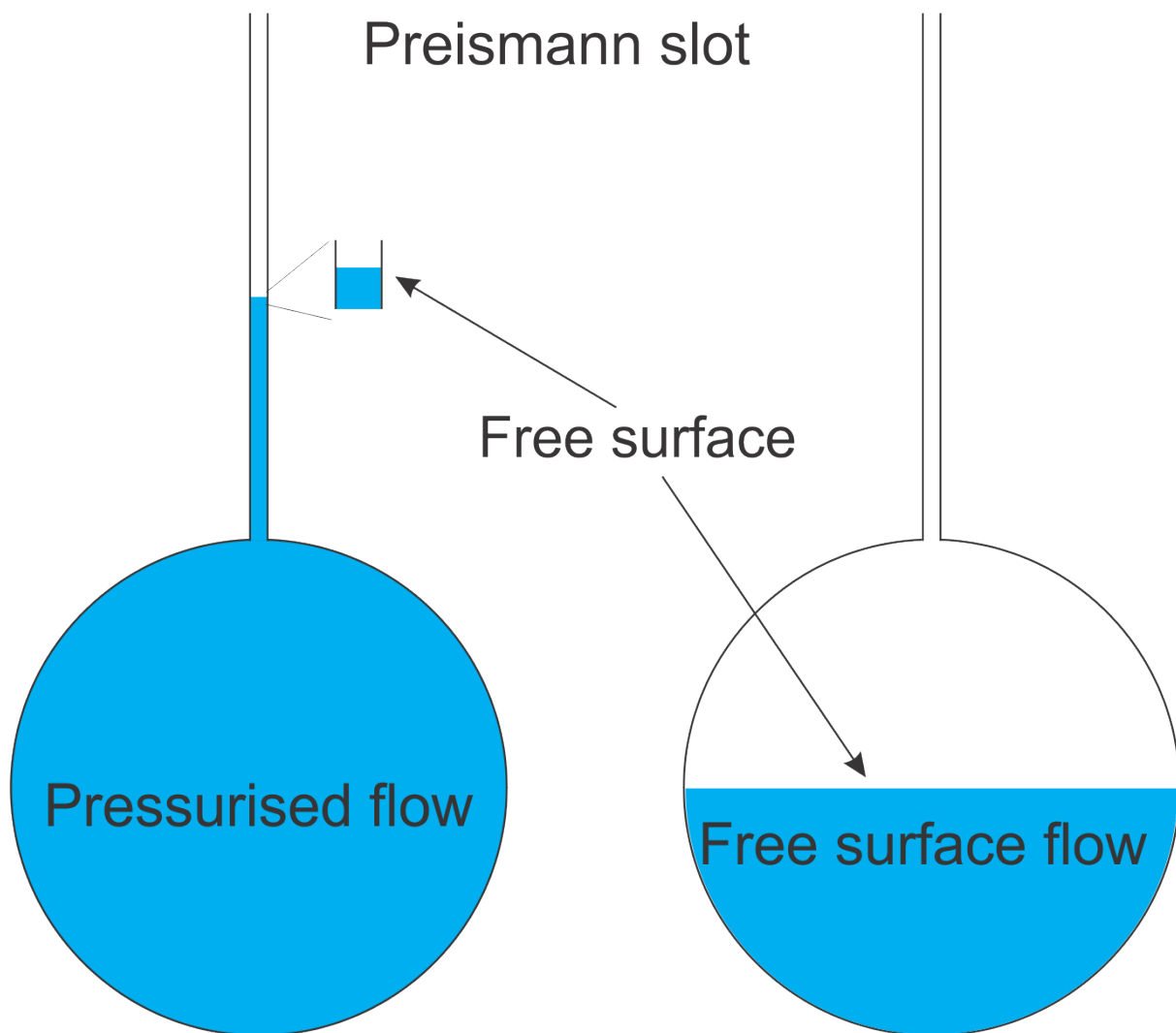
Figure 4: The use of a Preissmann slot enables use of the same set of equations for conduits with free surface flow and conduits with pressurised flow.

714
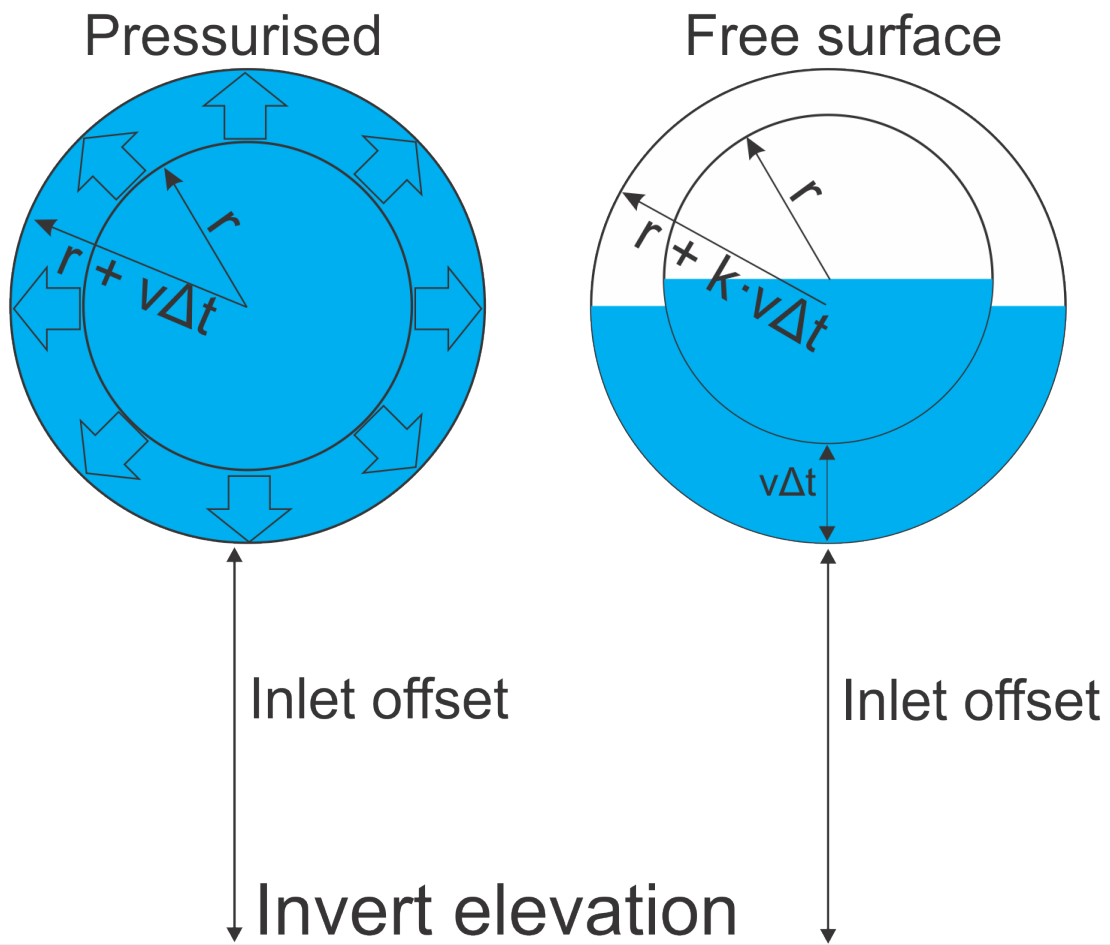
Figure 5: Growth of a conduit with pressurised flow and a conduit with free surface flow. *r* is radius, *k* is the fraction of wetted perimeter, *v* incision (growth) rate.

718
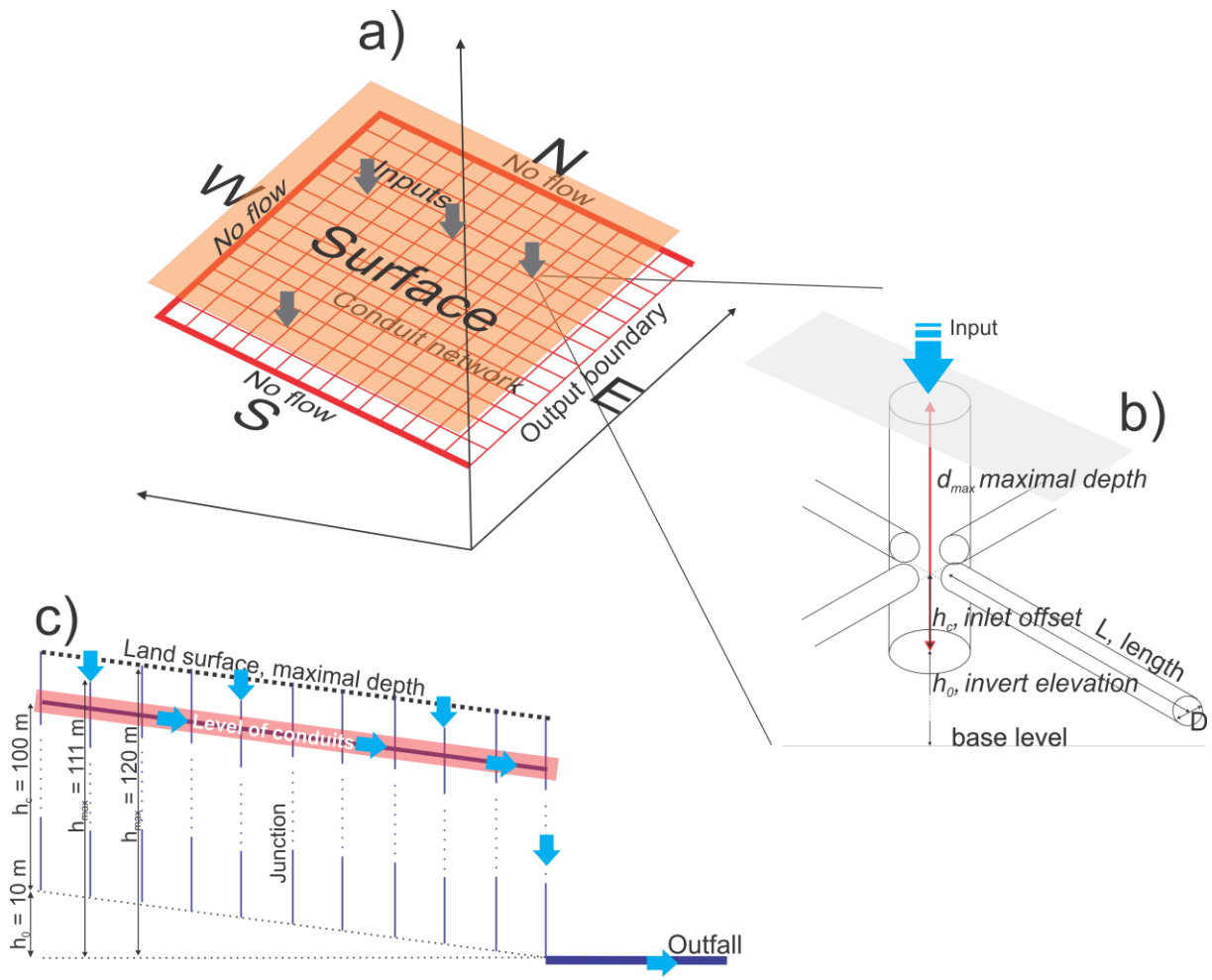
719

720 Figure 6: The model structure for the Low-dip network. a) A conduit network with discrete
721 water inputs, marked by arrows. Boundaries are denoted geographically. Outputs are along
722 the E boundary. b) Geometry and parameters of a junction. c) The side view of the model,
723 also showing a large conduit connecting E junctions to an outfall.

724

725
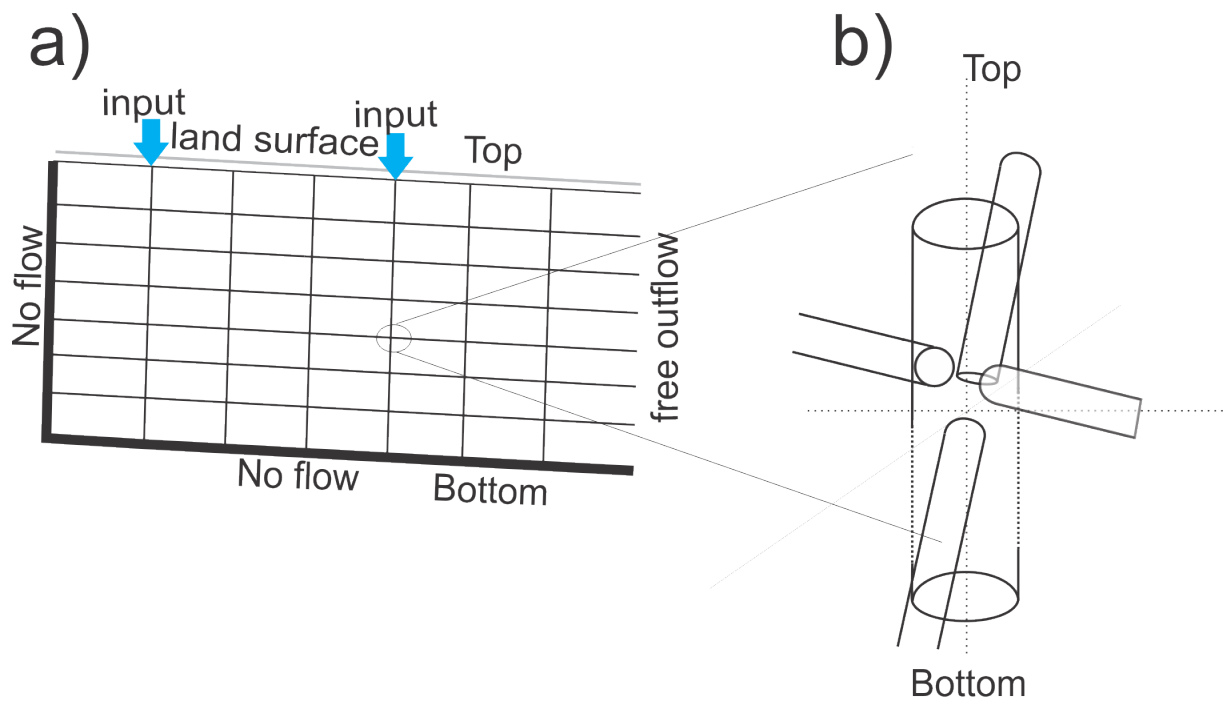
Figure 7: The model structure for the High-dip scenario. a) The slope of the network is 0.99 in
from top to bottom and 0.1 from left to right. The right boundary is a seepage face with free
outflow. Inputs are on the top. b) Junction geometry: high-dip ("vertical") conduits are
positioned below the low-dip ("horizontal") conduits.

730
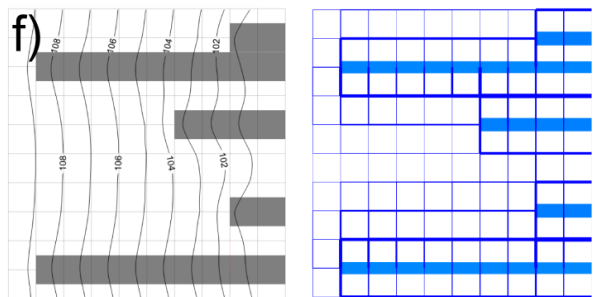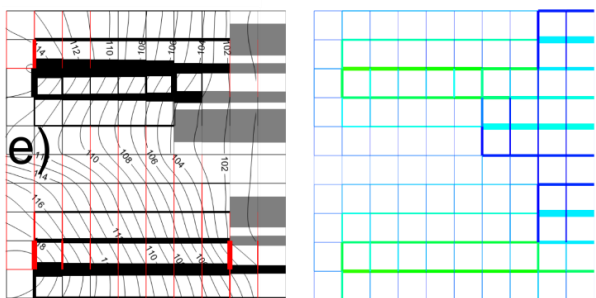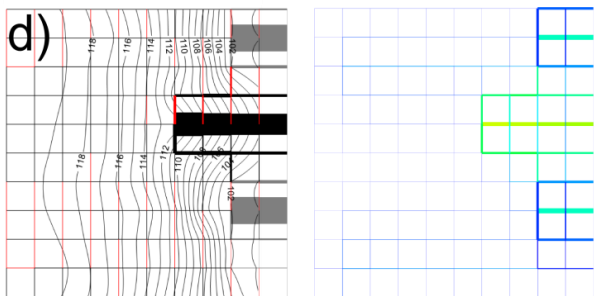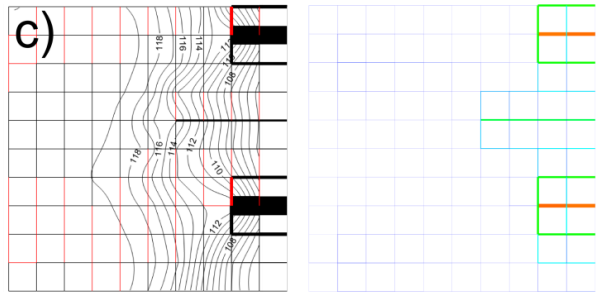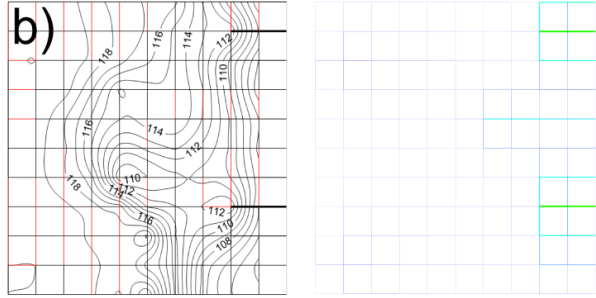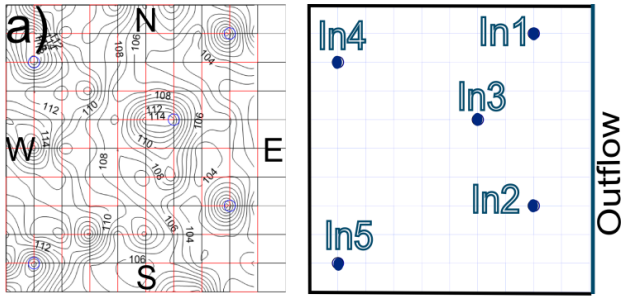
732   Figure 8: Six snapshots of the evolution of Low-dip network with uniform initial diameters
733   and inlet offsets. Left: flow rates (width) and flow direction (Red = flow towards E or towards
734   N, Black/Grey = flow towards W or towards S). Right: diameters (width) and widening rates
735   (colour). The codes below show thicknesses, flow rates and widening rate. The values at the
736   bar codes correspond to the thickest lines in the flow rate and diameter bars and to the
737   warmest colour in the bar for the widening rate. The scales are linear with the thinnest lines
738   and dark blue colours representing no flow, no widening the and smallest initial diameter.

739
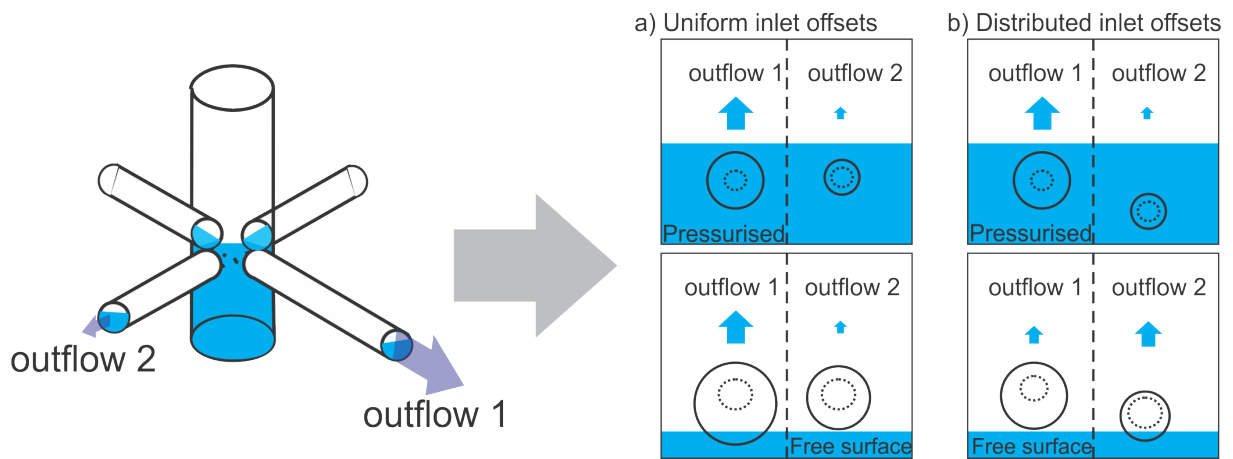
Figure 9: Left: the geometry of a junction. Right (a and b): Scheme of two outflows during pressurised flow (top) and free surface flow (bottom). a) initial inlet offsets for both outflows are equal. b) Initial inlet offset of outflow 2 is smaller so that the outflow has a lower elevation. Blue arrows indicate the amount of flow drained by each outflow, and the blue shading indicates the water table.

748
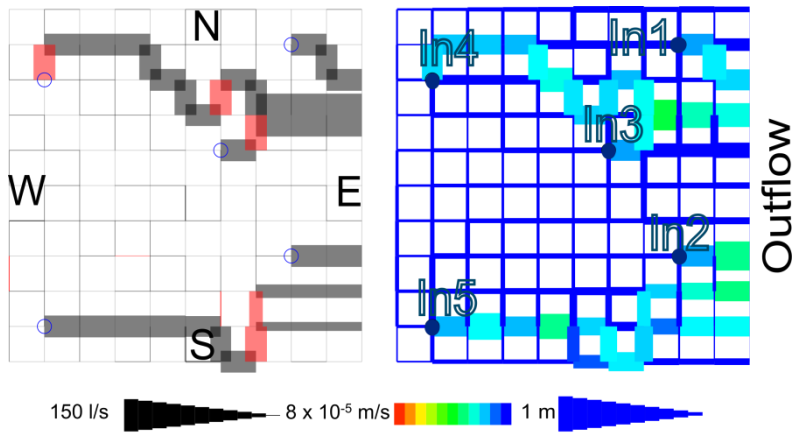
749

750 Figure 10: A network with uniform initial diameters and initial inlet offsets randomly
751 distributed within vertical span of 1 m.

752

753
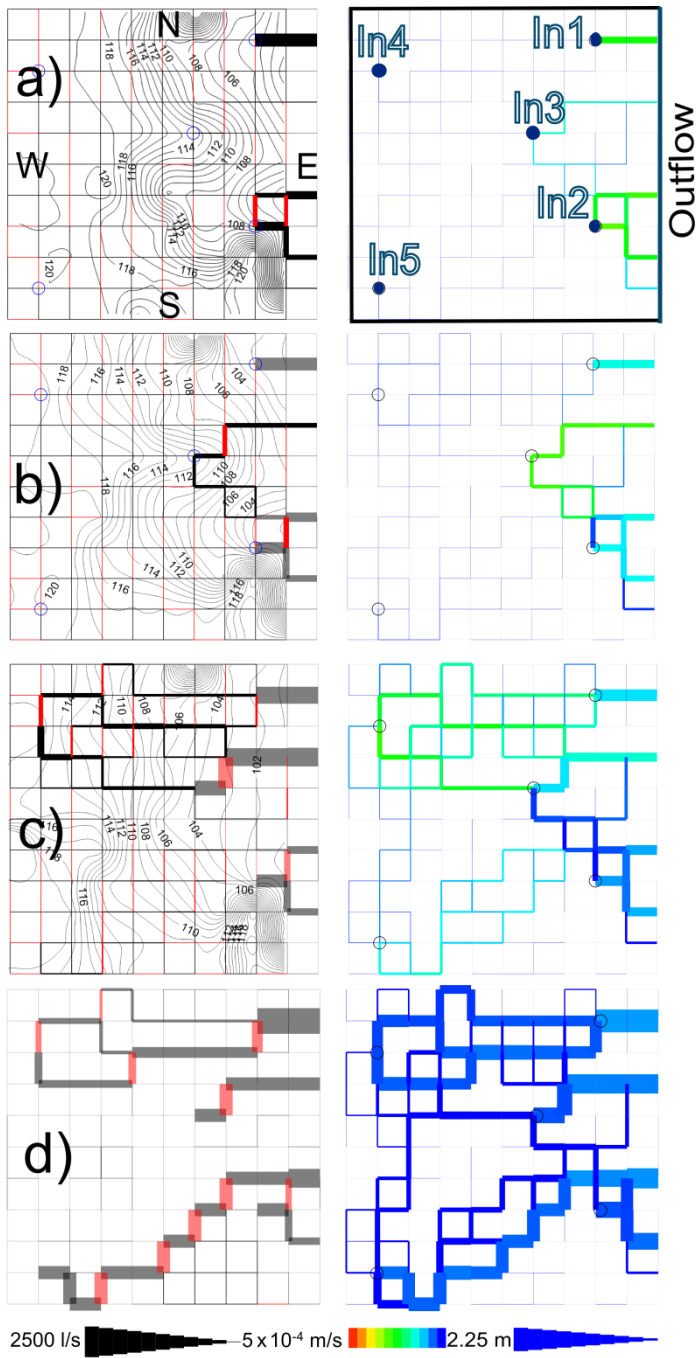
Figure 11: Evolution of a Low-dip network with randomly distributed initial diameters.

755
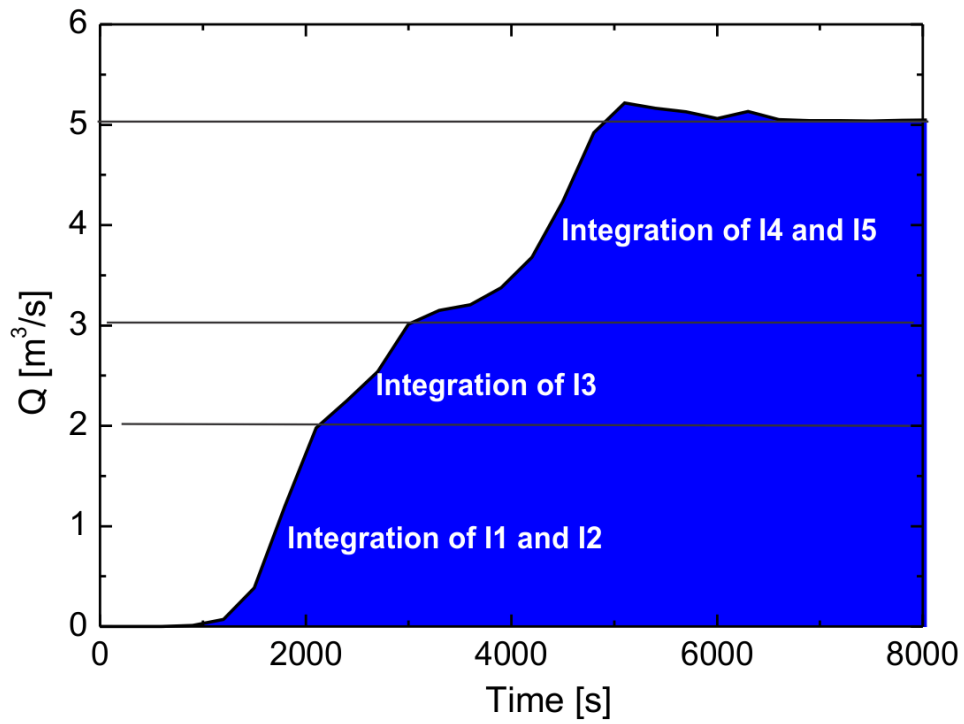
Figure 12: The time evolution of total discharge from the network in Fig. 11.

756

757

758
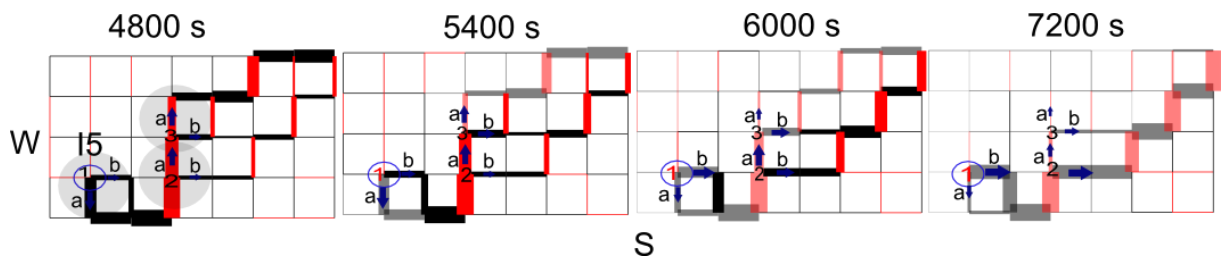
759

760 Figure 13: Evolution of SW edge of the network in from Fig. 11 before and after transition to
761 free surface flow.

a)

b)

pressurised   Δh $\updownarrow$

free surface

a

b

$v_a > v_b$

α a

b

α

$v_b > v_a$
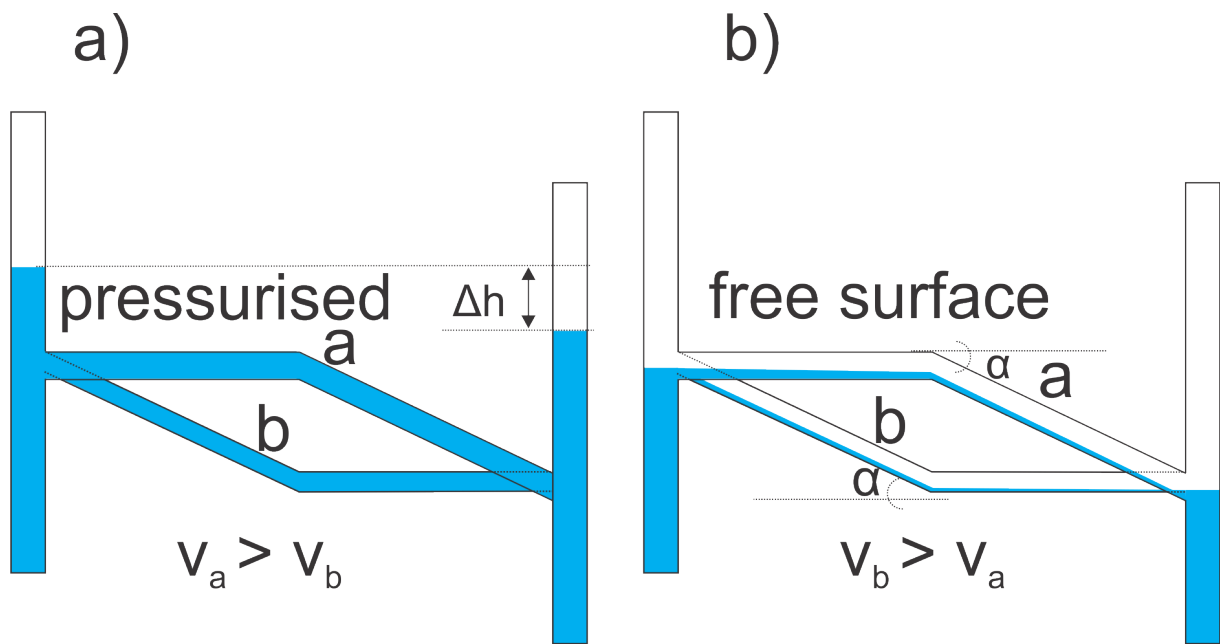
Figure 14: Distribution of flow between two pathways depends on the flow resistance when the flow is pressurised. The pathway *a* has with lower flow resistance grows faster. After the transition to free surface flow, the pathway *b* with higher exit slope from the junction can capture more flow and incise faster.

768

769
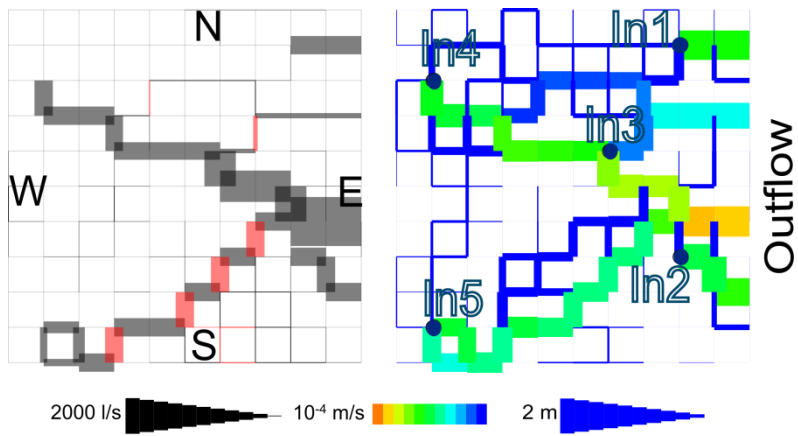
Figure 15: Quasi-stable state of network with same structure as presented in Fig. 11, but the plane of the network is additionally tilted from N to south, for 0.3 m per node
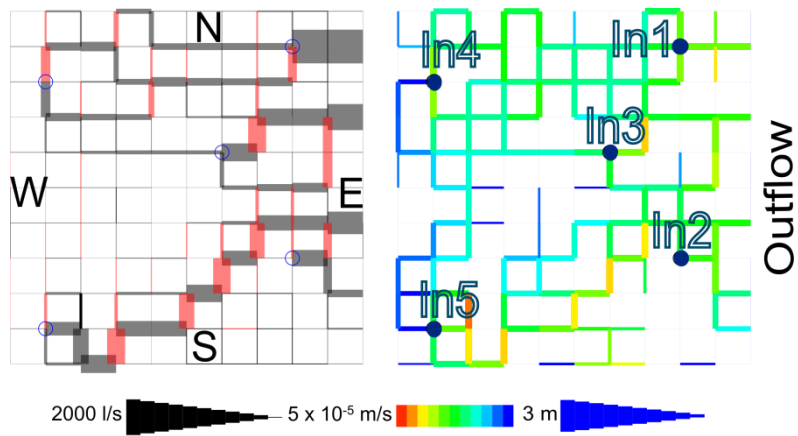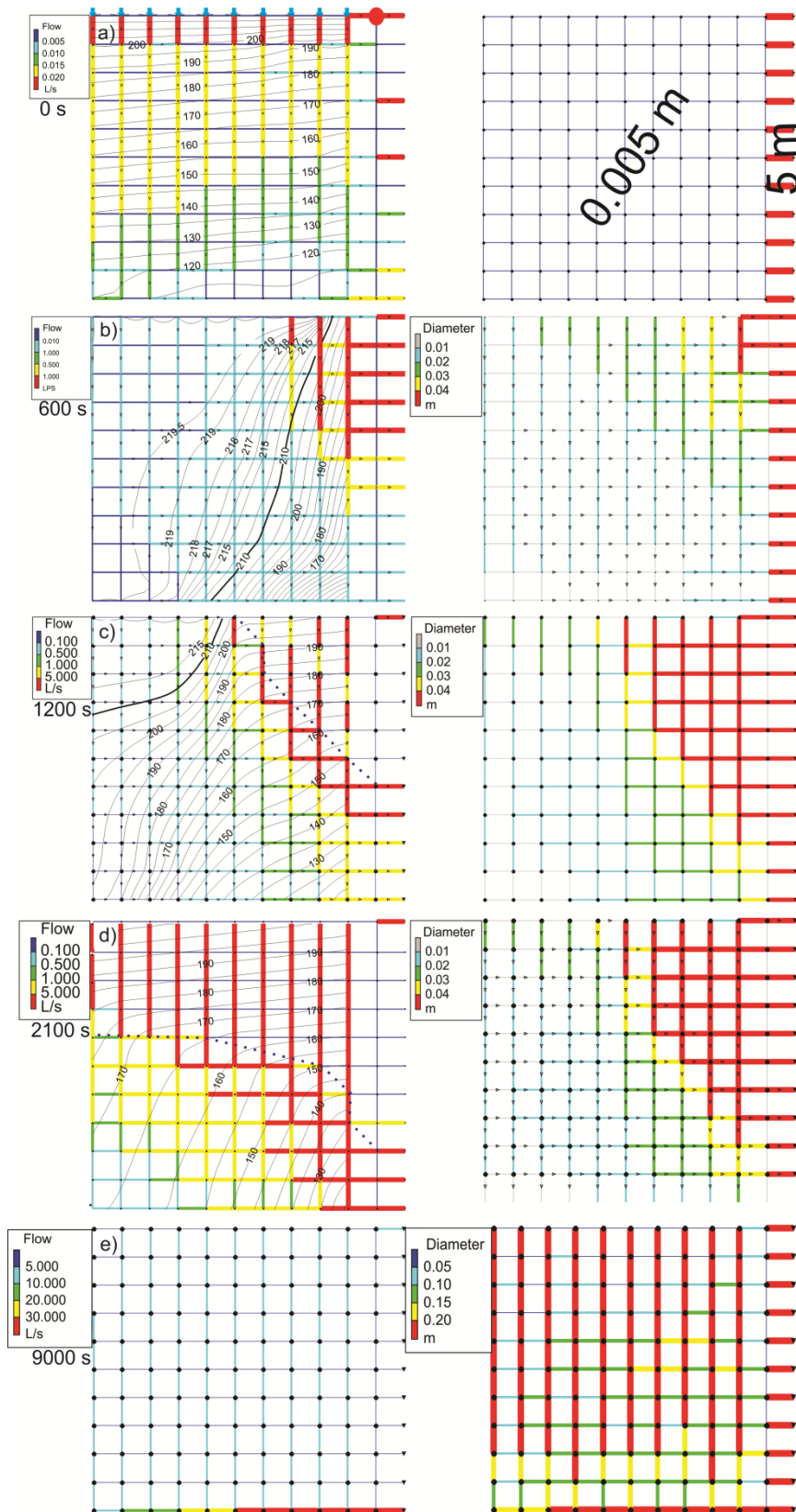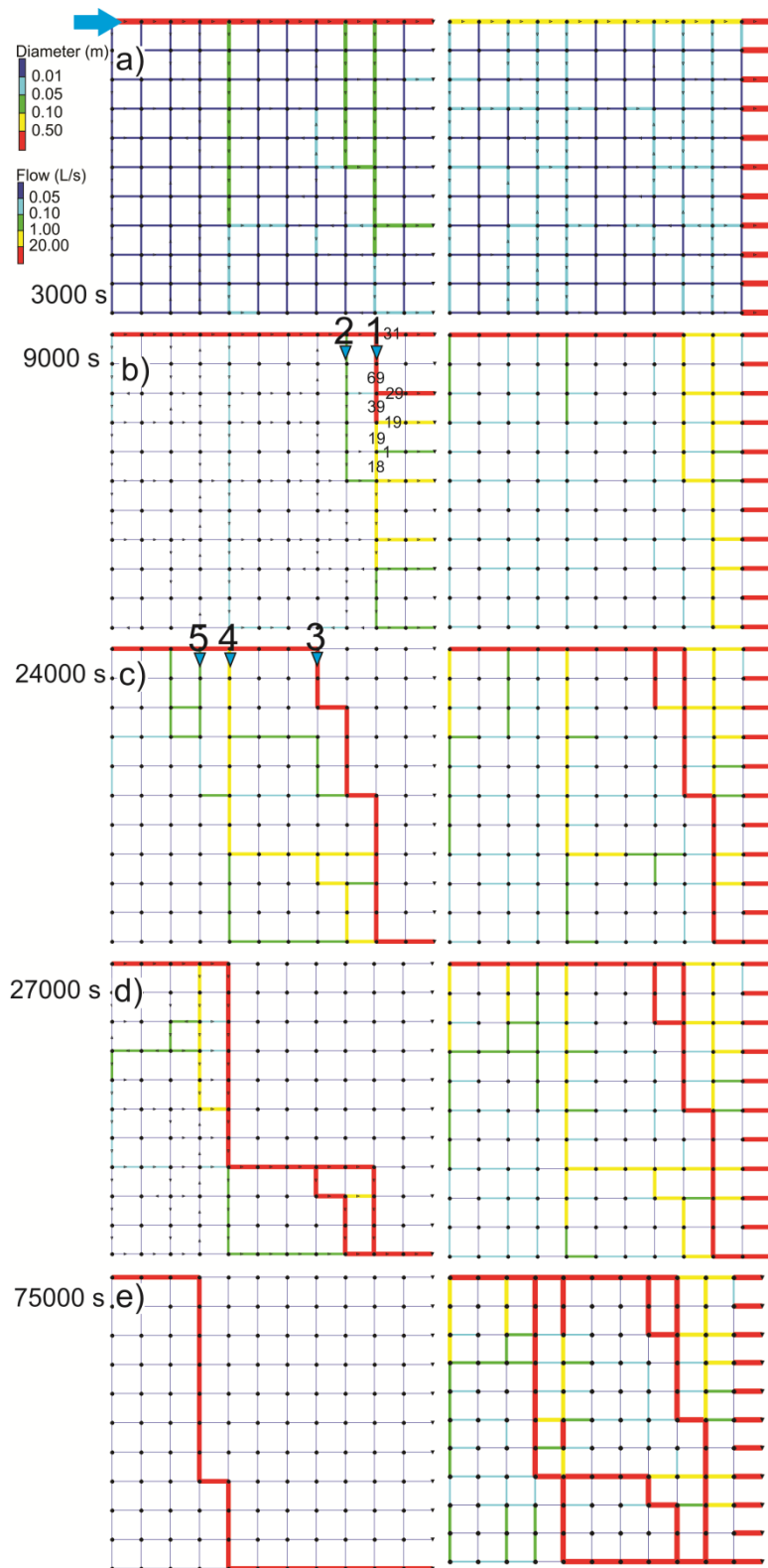
Figure 16: Quasi-stable state for the same scenario as in Fig. 11 with dissolution kinetics for limestone.

Figure 17: Evolution of homogenous sub-vertical network. Blue arrows on Fig. 17a denote inputs. Isolines and values present the hydraulic potential [m]

Figure 18: High-dip network with random initial distribution of conduit diameters. Flow enters at the top-left edge of the network as pointed by a blue arrow. Values on Fig. 18b show flow rates along the selected individual conduits
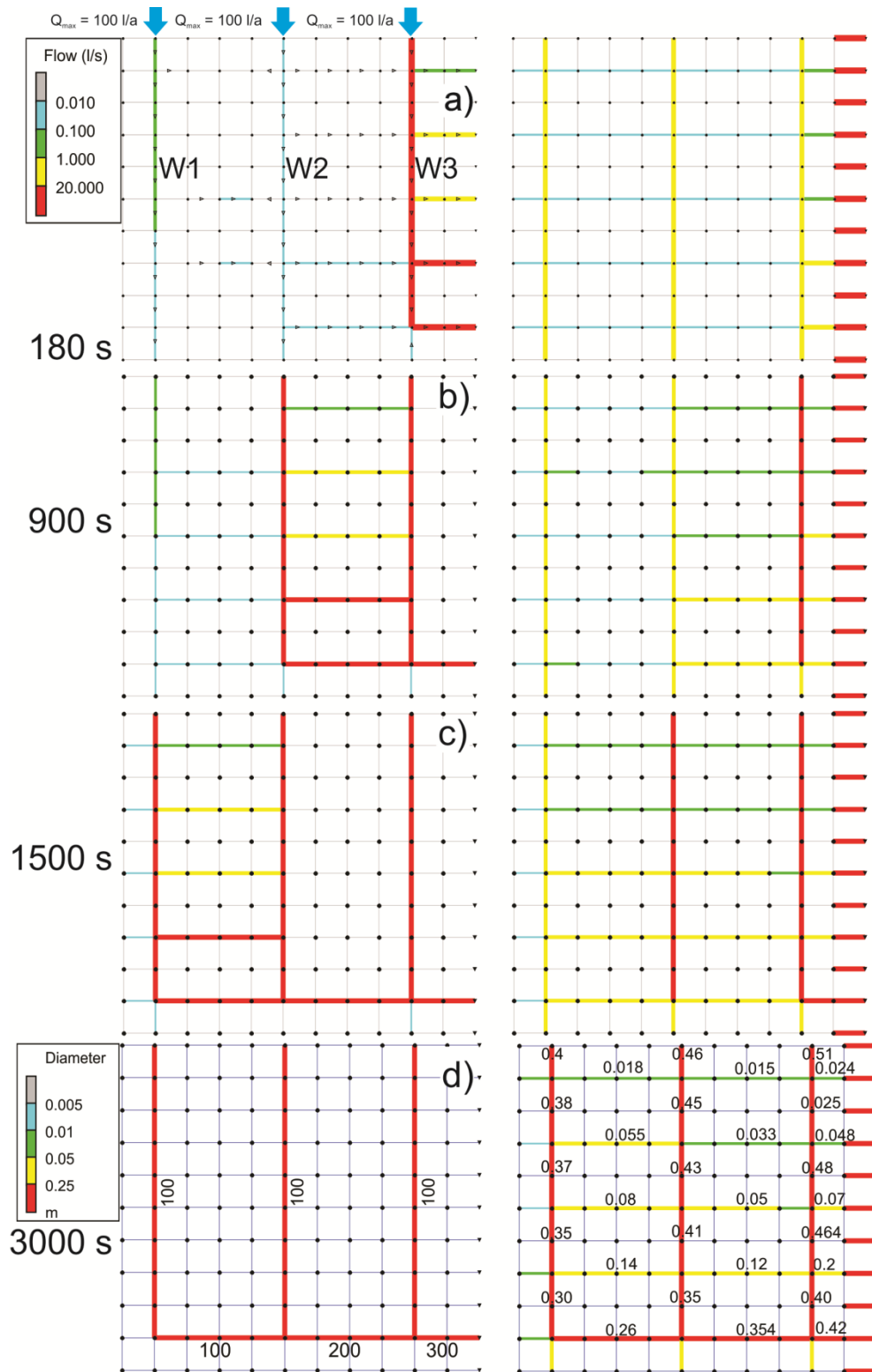
Figure 19: High-dip network with three prominent conduits (wells), marked by W1 to W3. A recharge of 100 l/s is available to the prominent conduits.